Good's Buffer Ionic Liquids as Relevant Phase-Forming Components of Self-Buffered Aqueous Biphasic Systems

Mohamed Taha[#], Maria V. Quental[#], Francisca A. e Silva, Emanuel V. Capela, Mara G. Freire, Sónia P. M. Ventura, and João A. P. Coutinho*

CICECO-Aveiro Institute of Materials, Department of Chemistry, University of Aveiro, 3810-193 Aveiro, Portugal

Abstract

BACKGROUND: Self-buffered aqueous biphasic systems (ABS) are prepared with ionic liquids (ILs) based in Good's buffers (GB-ILs) and used to purify proteins.

RESULTS: A set of new GB-ILs based on the tetrabutylphosphonium cation ($[P_{4444}]^+$) was here synthesized and characterized. The self-buffering behaviour of the GB-ILs was asserted by measuring their protonation constants by potentiometry. These ionic liquids display self-buffering characteristics as well as a low toxicity towards the luminescent bacteria *Vibrio fischeri.* The ability of the GB-ILs to form ABS with the potassium citrate salt was investigated. These systems were then evaluated to extract and purify BSA from bovine serum samples. Extraction efficiencies of 100 ± 5 % of BSA to the GB-IL-rich phase were obtained in a single-step. In addition, good recovery yields (59.4 ± 0.8 % to 80.1 ± 0.7 %), and purity levels of BSA (75.0 ± 0.3 % to 92 ± 1 %) were also achieved. The BSA secondary structure in the aqueous IL–rich solutions was evaluated through infrared spectroscopic studies revealing the protein-friendly

[#] both authors contributed equally for the development of this work

*Corresponding author. Fax: +351 234 370 084.
E-mail: jcoutinho@ua.pt (J.A.P. Coutinho).

This article has been accepted for publication and undergone full peer review but has not been through the copyediting, typesetting, pagination and proofreading process, which may lead to differences between this version and the Version of Record. Please cite this article as doi: 10.1002/jctb.5222

nature of the synthesized GB-ILs. Dynamic light scattering (DLS), "COnductor-like Screening MOdel for Real Solvents" (COSMO-RS), and molecular docking studies were finally carried to better understand the main driving forces of the extraction process.

CONCLUSION: The results obtained show that GB-IL based ABS can be prepared and used for protein purifications, with the GB-ILs showing a stabilizing effect on the protein.

KEYWORDS: Good's buffer ionic liquids, aqueous biphasic systems, Microtox, *Vibrio fischeri*, bovine serum albumin, purification, stability.

Introduction

Aqueous biphasic systems (ABS) are more benign alternatives to replace the conventional liquid–liquid extractions using organic volatile solvents aiming the efficient separation of biomolecules, in which proteins and enzymes are included [1, 2]. ABS are claimed as greener extraction techniques, minimizing the consumption of volatile organic solvents, which could be not only harmful to the environment and human resources, but also for proteins since they could cause their denaturation [3]. Several techniques such as electrophoresis, membrane separation, gel filtration, and affinity chromatography, were adopted in protein separation. However, they are some of the most expensive processes and consequently, are associated to several limitations, namely concerning their scale-up [4]. Traditional ABS consist of aqueous solutions of two polymers (e.g. polyethylene glycol and dextran) or a polymer and a salt. They have been established as an economical method making part of diverse downstream processes. These are claimed as methods exhibiting low-energy consumption, high performance, high

biocompatibility and suitability for large scale production. Consequently, the ABS processes have been extensively studied for the separation and purification of different biological products.

As promising substitutes for conventional organic solvents, ionic liquids (ILs) have become ubiquitous in the recent literature, due to their diverse properties, which are responsible for them to be useful in a large plethora of different applications [5, 6]. ILs are salts composed of a bulky, unsymmetrical organic cation and an inorganic or organic anion, which have a melting point below 100 °C. The wide structural diversity of ILs allows to adjust their properties, which consequently could improve the protein stability and activity [7-10]. On the other hand, a variety of hydrophilic ILs was found to form ABS when mixed with aqueous solutions of inorganic or organic salts, [5, 11-13] and proved to be efficient in the separation of proteins and enzymes [4, 14-29]. Moreover, and behind the efficiency of IL-based ABS as separation techniques, their many advantages over the conventional polymer-based systems, such as their lower viscosity and a higher difference in the phases' polarity, [4, 14-29] makes them a more attractive purification tool. IL-based ABS have been applied as purification techniques of a large range of macromolecules, these including enzymes like horseradish peroxidase (HRP), *Thermomyces lanuginosus* lipase, *Candida antarctica* lipase A, and *Candida antarctica* lipase B [21, 23, 30, 31], and proteins, namely BSA, cytochrome *c*, myoglobin, ovalbumin, hemoglobin, trypsin, cytochrome c, γ-globulins, among others [4, 14-20].

When considering the previously reported works, it is clear that IL-based ABS provide a higher extraction efficiency regarding proteins if compared with the most conventional polymeric systems. Moreover, some parameters were already defined as important conditions driving the migration of proteins, namely the potential formation of aggregates, or some particular interactions, like electrostatic, dispersive and hydrogen-bonding interactions [4, 14-29]. In the studies

reported in the last two decades, phosphate salts are still the most applied as salting-out agents. The phosphate buffer has been used to adjust the pH of the systems considering some specific proteins/enzymes and ABS [32-34]. However, and contrarily to the pH control by means of the added salt, buffered IL-based ABS can be created with ILs with self-buffering characteristics. For this purpose, we and the MacFarlane's group[35] recently developed a series of self-buffering and biocompatible ILs (Good's buffer ionic liquids, GB-ILs) in which five Good's buffers (GBs, namely Tricine, TES, MES, HEPES, and CHES) acted as anions and 1-ethyl-3-methylimidazolium ($[C_2mim]^+$), alkyllammonium ($[N_{nnnn}]^+$), and cholinium ($[Ch]^+$) acted as cations [36-38]. GBs were considered because they are *N*-substituted glycine or taurine compounds that are frequently used in different fields of application [39], which includes diverse biological systems. To expand this range of available GB-based ABS and to better understand their potential in separation processes, in this work, five new GB-ILs with self-buffering characteristics were synthesized by the conjugation of a wide variety of GB's anions and the tetrabutylphosphonium cation ($[P_{4444}]^+$). These were characterized in terms of their toxicity against the luminescent bacteria *Vibrio fischeri* [40], and further used to form GB-IL-based ABS with the biodegradable potassium citrate salt. The phosphonium cation ($[P_{4444}]^+$) was selected because it has an enhanced aptitude to form ABS [41], and thus lower amounts of phase-forming components will be required to create two-phase systems. After the determination of the corresponding phase diagrams, the BSA partition between both aqueous phases was evaluated and compared with that of tetrabutylphosphonium chloride ($[P_{4444}]Cl$). Moreover, and having determined and optimized the weight compositions to promote the complete migration of BSA towards the GB-IL-rich phase, the purification of BSA from a bovine serum sample was evaluated. The stability of BSA was also addressed and the molecular-level mechanisms

controlling the BSA extraction to the IL-rich phase were ascertained by COSMO-RS and molecular docking studies. The chemical structure of $[P_{4444}]Cl$ and the GB-ILs prepared in this work are depicted in Figure 1 (the synthetic pathway to prepare the latest is shown in Figure S1 in the Supporting Information).

Materials and Methods

Materials

N-[tris(hydroxymethyl)methyl]glycine (Tricine, purity > 99 wt%), 2-[(2-hydroxy-1,1-bis(hydroxymethyl)ethyl)amino]ethane sulfonic acid (TES, purity > 99 wt%), 2-(N-morpholino) ethanesulfonic acid (MES, purity > 99 wt%), 2-[4-(2-hydroxyethyl)piperazin-1-yl]ethanesulfonic acid (HEPES, purity > 99.5 wt%), 2-(cyclohexylamino)ethanesulfonic acid (CHES, purity > 99 wt%), and $[P_{4444}][OH]$ (45 wt% in water), were purchased from Sigma–Aldrich. Sodium hydroxide pellets were supplied from Eka Chemicals. BSA (fraction V) was obtained from Acros Organics. Methanol (HPLC grade, purity > 99.9 wt%) was obtained from Fisher Scientific (UK). Acetonitrile (purity > 99.7 wt%) was supplied from Lab-Scan (Ireland). Purified water passed through a reverse osmosis and a Milli-Q plus 185 water purifying system was used in all experiments. Sodium nitrate (purity > 99.5 wt%) was obtained from Himedia Labs. Potassium nitrate (purity > 98.0), nitric acid (65 wt%), and potassium hydrogen phthalate (purity > 99.8) were purchased from Panreac (Barcelona, Spain). The bovine serum sample used was obtained from Sigma-Aldrich (B9433 Sigma), USA, sterile-filtered and stored at −20 °C.

Synthesis and characterization of GB-ILs

The synthesis of the GB-ILs tested in this work follows the same standard protocols described elsewhere [42]. Briefly, an aqueous solution of $[P_{4444}][OH]$ was added drop-wise to a GB aqueous solution with a slight equimolar excess. The solution was stirred at room temperature during 12 h; then, the reaction mixture obtained was evaporated at 60 °C under vacuum. A mixture of acetonitrile and methanol (1:1) was added to the viscous liquid previously obtained, stirred vigorously at room temperature for 1 h until the precipitation of the unreacted buffer, which was posteriorly removed by filtration. The solvent (acetonitrile + methanol) was evaporated and the GB-ILs were dried under vacuum (~10^{-3} mbar) for 3 days at room temperature (25ºC). The water content of each GB-IL prepared (less than 0.05 wt %) was measured by Karl–Fischer coulometer (Metrohm Ltd., model 831). The chemical structures of the GB-ILs were confirmed by ^{1}H and ^{13}C NMR spectroscopy (Bruker AMX 300) operating at 300.13 and 75.47 MHz, respectively. The melting points of GB-ILs were measured by differential scanning calorimetry (DSC), with a Perkin Elmer DSC-7 instrument (Norwalk, CT), at a heating rate of 5 °C.min^{-1} and under a N_2 flow of 40 mL·min^{-1}. These data (NMR data and melting points) are presented in Table S1 in the Supporting Information file.

Potentiometric titrations

pH-potentiometric apparatus: The pH-potentiometric measurements were carried out in a 70 cm^{-3} double-walled glass vessel using an automatic titrator (Metrohm 904) equipped with a 801 magnetic stirrer, Dosino buret model 683, and a pH glass electrode (Metrohm 6.0262.100) with a precision of ± 0.001. The temperature of the titration cell was controlled at 25.0 ± 0.1 ºC by a thermostatic water bath. The titration cell was equipped with a lid with various openings for insertion of the electrode, burette tip, Pt 1000/B/2 (Metrohm 6.1114.010), and gas inlet and

outlet. The titroprocessor was coupled to a personal computer and the titration software Tiamo 2.3 was used to control and record the titration process.

pH profiles procedure: 10 mL of GB-ILs (0.05 M) were titrated with 0.1 mol·dm^{-3} of NaOH/HCl under continuous magnetic stirring. The pH electrode was calibrated using three standard buffer solutions of pH 4.01, 7.00, and 9.21.

Determination of protonation constants of GB/GB-ILs: The glass electrode was calibrated considering the hydrogen ion concentrations instead of activities, by means of a strong acid-strong base titration. In this titration, 2 cm^{-3} of 0.1 M of HNO_3 and 50 cm^{-3} of 0.1 M of a KNO_3 solution were titrated with a 0.1 M of carbonate-free NaOH solution. The concentration of NaOH was determined by standardization with potassium hydrogen-phthalate. The water purified was degassed under vacuum using a rotary evaporator at 70 ºC and cooled under a stream of nitrogen. The titration cell was kept under a small positive pressure of nitrogen gas to eliminate the effect of atmospheric carbon dioxide. The nitrogen gas was purged for 15 min before starting the titration to expel any dissolved oxygen or carbon dioxide present. The values of volume added (cm^{-3}) and electrode potential (mV) were analyzed with the GLEE software [43]. This computer program uses a (non-linear) least-squares refinement to fit a modified Nernst equation, Eq. (1),

$$E = E^{\circ} + s \log[H^{+}] \quad (1)$$

where E refers to the potential of the glass electrode, E^{o} and s are the standard electrode potential and slope, and [H^{+}] is the hydrogen ion concentration.

In the acid region, the hydrogen ion concentration, T_H, is obtained from Eq. (2), that is, log[H+] = log(T_H).

$$T_H = \frac{a_H v_0 + \gamma b_H v}{v_0 + v_1 + v} \quad (2)$$

where a_H is the acid concentration (mol·dm^{-3}) and v_0 (cm^3) is the initial volume added to the titration vessel. b_H is the base concentration (mol·dm^{-3}) in the burette (with negative sign), and γ is a correction factor for the base concentration. v is the volume (cm^3) of base added from the burette, and v_1 (cm^3) is the volume of the electrolyte solution.

In the alkaline region, the hydrogen ion concentration, T_H, is given by Eq. (3), where log[H+] = -pK_w - log(-T_H), v_e^a is the volume (cm^3) at the acid equivalence point, and v_e^b is the volume (cm^3) at the alkali equivalence point.

$$T_H = \frac{a_H v_0 + \gamma \frac{v_e^a}{v_e^b} b_H v}{v_0 + v_1 + v} \quad (3)$$

The Gran plot was used to estimate the carbonate contamination in the titrant and a typical Gran plot is shown in Figure S2. The product of water pK_w = 13.778 at 25 °C and ionic strength I = 0.1 mol·dm^{-3} KNO_3 were maintained constant during the refinements [44].

Titrations for protonation constant calculations were performed by combining 0.003 M of HNO_3, 0.1 M of $NaNO_3$, and 0.001 M of GB/GB-ILs (total volume of 50 cm^3) and titrated with the NaOH solution under carefully controlled experimental conditions, as described in the glass electrode calibration procedure. Each titration was repeated at least three times (more than 100 data points for each one). The determination of the protonation constants were computed using the HYPERQUAD program (Version 2008) [45]. This computer program treats the protonation equilibria of ligand as overall association constants; e.g. the protonation equilibria of H_2A which can be expressed as:

$$H^+ + A^{2-} \Leftrightarrow HA^- \; ; [HA^-] = \beta_1 [H^+][A^{2-}] \quad (4)$$

$$2H^+ + A^{2-} \Leftrightarrow H_2A^- ;\ [H_2A^-] = \beta_2\ [H^+]^2[A^{2-}] \quad (5)$$

The stepwise acid dissociation constants of H_2A is given by:

$$H_2A \Leftrightarrow\ H^+ + HA^-\ ;\ [H_2A]\ = K_{a1}\ [H^+][HA^-] \quad (6)$$

$$HA^- \Leftrightarrow\ H^+ +\ A^{2-}\ ;\ [HA^-]\ = K_{a2}\ [H^+][A^{2-}] \quad (7)$$

Since pK_a = - log($1/K_a$), the $pK_{a's}$ values are given by $pK_{a2} = log\beta_1$ and $pK_{a1} = log\beta_2 - log\beta_1$.

Dynamic light scattering (DLS) measurements

The hydrodynamic radius (R_H) values of the protein were measured at different temperatures using a Zetasizer Nano ZS equipment (Malvern Instruments Ltd., UK). The average R_H was calculated from the scattering intensity data using the instrument software. The light source of the instrument is He-Ne laser light (4mW) with a wavelength (λ) = 633 nm, and the scattering angle were fixed at 173°. The instrument is provided with a thermostatic sampling chamber which controls the temperature in the range from 0 ºC to 90 °C. The samples were prepared with 20 mg·cm^{-3} of BSA in (0.05 and 0.5) M of GB/GB-ILs/[P_{4444}]Cl, and at pH= 7.4. The samples were incubated at 25 °C for 4 h to achieve the equilibrium. Around 1.3 cm^{-3} bubble free sample in a square glass cuvette (PCS8501) was used for the DLS measurements.

Infrared measurements

Attenuated total reflectance (ATR) Fourier transform infrared (FTIR) spectra of 30 mg BSA in (0.05 and 0.5) M of GB/GB-ILs/[P_{4444}]Cl solutions were measured using an ABB MB3000 FTIR spectrometer equipped with PIKE MIRacle™ and a single refection diamond/ZnSe crystal plate.

The spectral region was 400-4000 cm^{-1} with a resolution of 4 cm^{-1} and 100 scans. At least 5 measurements were performed for each sample. Second-derivative spectra of the amide I (~1652 cm^{-1}) region were used as peak position guides for the Gaussian curve-fitting analysis. The second-derivative and the curve fitting were done using PeakFit v4.0 (AISN software Inc.). The relative amount of α-helices, β-sheets, and turns was estimated by calculating the areas of the bands assigned to a particular substructure.

Phase diagrams and tie-lines

The binodal curve of each phase diagram was determined through the cloud point titration method at 25 (± 1) °C and at atmospheric pressure, as detailed elsewhere [42]. The tie-lines (TLs) of each phase diagram, including the mixtures compositions for which the extraction of BSA was carried out, were determined by a gravimetric method originally described by Merchuk et al [46]. In this section, the same procedures described in literature [42] were adopted.

Extraction of commercial BSA

The biphasic systems used for the extraction of BSA were gravimetrically prepared at a fixed common mixture composition: (39.4 ± 0.7) wt % of GB-IL/IL + (15.1 ± 0.9) wt % of salt + water. The aqueous solution added to complete the mixture composition contained BSA at a concentration of *circa* 0.5 $g \cdot L^{-1}$. BSA was quantified by SE-HPLC and further details can be found elsewhere (Taha et al., 2015b). The wavelength used to quantify the BSA was set at 280 nm whereas the retention time of BSA in the HPLC chromatograms was found to be 9.31 min within an analysis time of 24 min, using the external standard calibration method in the range of 0.001 to 1 $g \cdot L^{-1}$ of BSA. In this work, three ABS of each IL were prepared and three samples of

each phase were properly quantified. Blank controls were always used to ascertain on the rotation times of the ABS phase-forming components.

The extraction efficiency of BSA, EE_{BSA} (%), was calculated to evaluate the success of each ABS to the extraction of BSA. This parameter describes the ratio between the amount of protein quantified in the IL-GB-rich phase and the sum of the amount of the protein in both phases, as defined in Eq. (8):

$$EE_{\mathrm{BSA}}\ (\%) = \frac{w_{BSA}^{IL}}{w_{BSA}^{IL} + w_{BSA}^{Salt}} \times 100 \qquad (8)$$

where w_{BSA}^{IL} and w_{BSA}^{Salt} are the total weight of BSA in the GB-IL-rich and in the potassium-citrate-rich phases, respectively.

Purification of BSA from a bovine serum sample

After the study and optimization of the partition of commercial BSA, it was evaluated the use of the same systems for the purification of BSA from a bovine serum real sample. The same mixture point (ABS) was adopted and the bovine serum was diluted at 1:40 (v/v) in PBS before use. Each mixture was mixed using a Vortex mixer, centrifuged (10 min at 1000 rpm), in order to achieve the complete partition of the serum content between the two aqueous phases. After the phases' separation, the monomeric BSA and remaining proteins (mostly a BSA dimer) were quantified by SE-HPLC, as described in the previous section. The extraction efficiency was once again determined according to Eq. (8). Moreover, the recovery yield - Eq. (9) - and purity of the monomeric BSA (target macromolecule) - Eq. (10) - to the GB-IL-rich phase were also determined:

$$Y_{\mathrm{BSA}}\ (\%) = \frac{W_{\mathrm{BSA}}^{IL}}{W_{\mathrm{BSA}}^{\mathrm{initial}}} \times 100 \qquad (9)$$

$$P_{\mathrm{BSA}}\ (\%) = \frac{peak\ Area^{IL}_{\mathrm{BSA}}}{total\ peak\ Area^{IL}_{\mathrm{proteins}}} \times 100 \quad (10)$$

where $W^{\mathrm{IL}}_{\mathrm{BSA}}$, $W^{\mathrm{initial}}_{\mathrm{BSA}}$, $peakArea^{IL}_{\mathrm{BSA}}$ and the $total\ peak\ Area^{IL}_{\mathrm{proteins}}$ are, respectively, the weight of monomeric BSA in the GB-IL-rich phase, the weight of monomeric BSA in the initial mixture (bovine serum), the peak area of the monomeric BSA and the total area of all peaks corresponding to all proteins present in the bovine serum determined by HPLC in the GB-IL-rich phase. All extractions were carried out in duplicate.

Computational details

COSMO-RS modelling: The detailed theory on ‘‘Conductor-like Screening Model for Real Solvents’’ (COSMO-RS) was described in detail by Klamt [47]. This model integrates concepts from quantum chemistry, continuum solvation model (COSMO), electrostatic interaction and extends to statistical thermodynamics, which are recurrently used for predicting the thermodynamic properties of fluids and liquid mixtures. COSMO-RS is used to analyse the electrostatic interaction (E_{misfit}(σ and σ′)), H-bonding (E_{HB}) and van der Waals (E_{vdW}) interaction energies of interacting species in terms of the screening charge densities (σ, σ') of the respective surface segments - Eqs (11-13) [48],

$$E_{MF}(\sigma, \sigma') = a_{\mathrm{eff}} \frac{\propto'}{2} (\sigma + \sigma')^2 \quad (11)$$

$$E_{\mathrm{HB}} = a_{\mathrm{eff}} c_{hb} min(0, \sigma\sigma' + \sigma_{hb}^2) \quad (12)$$

$$E_{\mathrm{VdW}} = a_{\mathrm{eff}} (\tau_{vdW} + \tau'_{vdW}) \quad (13)$$

where a_{eff} refers to the effective contact area, α′ is a general constant, c_{hb} is the strength coefficient, σ_{hb} represent the polarization charge density threshold for hydrogen bond, and τ_{vdW} and τ'_{vdW} are the element-specific parameter for dispersion parameters. The 3D distribution of the polarization charges, σ, of each molecule is converted into a surface composition function, named as sigma profile (σ-profile), by the COSMO*therm* program version C30_1401 [49, 50]. The σ-profile depicts the surface charge density distribution on the molecular surface, which provides quantitative information about the polarity of the molecules [48, 49]. The σ-profiles of $[P_{4444}][GB]/[P_{4444}]Cl$ were computed at the RI-DFT BP/SVP level, as implemented in the TURBOMOLE 6.1 program package [51], and the interaction energies were calculated using the COSMO*therm* software version C30_1401.

Octanol-water partition coefficient calculation (log K_{OW}): The DFT/COSMO calculations of GBs were computed using the TURBOMOLE 6.1 program with RI-BP/TZVP method [51]. The logK_{OW} (octanol-water partition coefficients) values of all GBs were determined by the COSMO*therm* software, version C30_1401 [49, 50]. The K_{OW} is obtained through the computation of the ratio of the activity coefficient of the buffer at infinite dilution (γ_i^{∞}) in the water- and octanol-rich phases, as indicated in Eq. (14).

$$K_{OW,\,i} = 0.151\, K_{OW,\,i} = 0.1505 \frac{\gamma_i^{\infty,\,W}}{\gamma_i^{\infty,\,O}} \qquad (14)$$

where the superscripts "W" and "O" refer to the water-rich and the octanol-rich (0.726 mole fraction of octanol) phases, respectively.

QSAR-serum albumin binding model, logK(HSA): The molecular geometries of $[P_{4444}][GB]/[P_{4444}]Cl$ were first computed with the AM1 semi-empirical method with Polak-Rebiere algorithm to reach a 0.01 root mean square gradient as implemented in the HyperChem

(Version 8.0.7, Hypercube, Inc, USA, http://www.hyper.com) program. The COSMO files of these ILs were then obtained by single point calculations at the RI-DFT BP/SVP level using the TURBOMOLE 6.1 program package [51]. The QSAR-logK(HSA) values were computed using these COSMO files with the COSMO*therm* software, version C30_1401[49, 50].

Molecular docking: The molecular docking between BSA and the diverse $[P_{4444}][GB]$ ions was performed using the Auto-dock Tools vina 1.5.4 program [52] and the three-dimensional structures of BSA (PDB, 3v03) [53]. Further details can be found elsewhere [54]. The lowest binding model was searched out from 9 different conformers for each ligand based on the one with the lowest objective function, which includes electrostatic interactions, hydrogen bonding, short range vdW, and solvation energies terms.

Standard Microtox® liquid-phase assays

The luminescence inhibition of the marine bacteria *Vibrio fischeri* (strain NRRL B-11177) was measured after contacting with each $[P_{4444}][GB]$ at 15 ºC. The protocol followed in this work (81.9% standard test) is described elsewhere in detail [54]. Also in this work the effective concentration yielding 50% of inhibition of the bacteria luminescence (EC_{50}) along with the corresponding 95% confidence limits were determined through the Microtox® Omni™ Software version 4.1 [55], to evaluate the toxicity of each GB-IL.

Results and Discussion

The acid-base behavior of the novel GB-ILs

Good's buffers are zwitterionic compounds with two protonation states, the carboxylic/sulfonic (pKa_1) and the amino (pKa_2) groups. The first acidic sites of Good's buffers are released below

ca. pH 3.0, while the second protonation constants are included in the physiological pH region of pH 6 to 9. The pH-profiles of these GB-ILs were measured in aqueous solution (Figure 2a) to identify their buffering action, through which it is possible to show their buffering-like region, described by the moderate slope length appearing before the inflection point at high pH. Their buffer capacity is a measure of a buffer's ability to resist changes in pH upon the addition of an acid or base. Mathematically, the buffer capacity (β) is normally defined according to Eq. (15),

$$\beta = {}^{dC_b}\!/_{d(pH)} = -{}^{dC_a}\!/_{d(pH)} \quad (15)$$

where C_b and C_a, are the number of moles of strong base or acid added *per* liter. The buffer capacity of the GB-ILs in aqueous solution is shown in Figure 2b. From this figure, we can see that the buffer capacities of GB-ILs are relatively high and offer a wide range of pH values. The buffering regions of $[P_{4444}]$[MES], $[P_{4444}]$[TES], $[P_{4444}]$[HEPES], $[P_{4444}]$[Tricine], and $[P_{4444}]$[CHES], are 4.7–7.3, 6.2–8.7, 6.2–8.8, 6.6–9.7 and 7.7–10.7, respectively. The pH at the middle of the buffering region is equal to the pKa_2, and thus the buffering capacity is, at this point, the highest.

The (acid + base) equilibria of GBs and GB-ILs (e.g., MES and $[P_{4444}]$[MES], respectively) are represented in Figure 3. The pKa_1 and pKa_2 values of the investigated Good's buffers at 25 °C and the ionic strength of 0.1 M of $NaNO_3$, as well as the corresponding GB-ILs, are reported in Table 1. The pKa_1 values of MES, TES, and CHES, are here reported for the first time. The pKa_2 values obtained in this work are in good agreement with those found in the literature [56]. Representative potentiometric fitted profiles of MES and $[P_{4444}]$[MES] using the HYPERQUAD 2008 program [45] are shown in Figure 2a. The distribution diagrams of species computed with the HySS program [57] for MES and $[P_{4444}]$[MES] as a function of pH, are presented in Figure 2b. The

potentiometric profiles and distribution diagrams of the species for the other investigated GB/GB-ILs are given in Figure S3 in the Supporting Information. From the obtained results (potentiometric profiles and species distribution diagrams) it can be gauged that GB-ILs are more easily deprotonated than the corresponding GBs, as confirmed by the lower p*K*a values of the former (Table 1). It should be remarked that it was not possible to determine the pKa_1 value of [P_{4444}][TES] and [P_{4444}][CHES]. The observed decrease in the pKa_1 and pKa_2 values of GB-ILs can be attributed to a higher stabilization of their free conjugated bases by electrostatic interactions with the tetrabutylphosphonium cation.

To determine the optimum pH of a protein function, different buffers are used to maintain the solution buffer capacity. However, the available universal buffers are scarce and have drawbacks since their anions interact or chelate metal-ions. The biological buffers MES, HEPES, and CHES are compatible with systems containing metal ions due to their negligible affinity to metal ions, and thus they are used to formulate biocompatible universal buffers in aqueous solution (Figure 5). The universal Good's buffers composed of '[P_{4444}][MES] + [P_{4444}][HEPES] + [P_{4444}][CHES]' presents a linear behavior in the pH range from 5.5 to 10.5 and can be seen as a promising option.

ABS phase diagrams

The formation of an ABS depends on the IL type and its concentration, salt type and its concentration, temperature, and also very important the pH. The intensity of the phase-forming ability in each IL-based system relays on the basis of the complex and competing nature of the interactions occurring between the solutes (*i.e.*, ions from the inorganic salt and IL) and water or between the phase-forming components[58]. The phase diagrams provide information about the concentration of phase forming components needed for the design of purification processes using

ABS. The experimental data corresponding to the ternary phase diagrams determined in this work, as well as the respective correlations, are presented in Tables S2 and S3 in the Supporting Information. For all ABS studied, the top phase corresponds to the IL-rich aqueous layer while the bottom phase is salt enriched. Figure 6A depicts the phase diagrams obtained for several $[P_{4444}][GB]/[P_{4444}]Cl$ and $K_3C_6H_5O_7$ systems. Table S4 (Supporting Information) presents additional data regarding the phase diagrams description, namely tie-lines (TLs) and respective tie-line lengths (TLL). The $[P_{4444}]$ cation is already known for its high ability to form ABS with different salts, which easily justifies the easy formation of ABS with all the GB-ILs prepared in this work. The formation of ABS using these GB-ILs is driven by the low affinity of the phosphonium cation for water, since it has a highly positive shielded charge that is surrounded by four hydrophobic alkyl chains. The smaller the affinity for water and/or the higher hydrophobic nature of the IL, the more prone it is to be salted-out [59] by the other phase former, in this case, the potassium citrate salt. Since potassium citrate is a strong salting-out salt [60], it has a higher affinity for water and thus the GB-ILs are strongly salted-out from the aqueous solution and create a two-phase system. In Figure 6B, the binodal curves are plotted on a molality scale, together with the data for the ABS composed of $[P_{4444}]Cl + K_3C_6H_5O_7$ obtained from literature [61] for comparison purposes. It can be seen from Figure 6B that the phase-forming ability of all GB-ILs is higher than $[P_{4444}]Cl$, meaning that lower amounts of both GB-IL and salt are required to form ABS. If compared to more traditional and commercially available ILs, these have the crescent benefits of reducing the cost and simultaneously increase the biocompatible nature of these systems when applied as purification/fractionation platforms. The GB-IL anions ability to form ABS, for instance at 1.0 $mol \cdot kg^{-1}$ of $K_3C_6H_5O_7$ follows the order: $[CHES]^- > [MES]^- > [HEPES]^- > [TES]^- > [Tricine]^-$. At a first glance, this trend can be interpreted in the light of each

anion chemical structure (*cf.* Figure 1): *i)* the [Tricine] and [TES] anions' weakest ABS formation ability is a consequence of the presence of three hydroxyl groups that enhance their hydrogen-bonding capacity with water, turning the salting-out process by the citrate-based salt a more difficult task; *ii)* $[HEPES]^-$, with one hydroxyl group, is ranked in an intermediate position; *iii)* and finally $[MES]^-$ and $[CHES]^-$, with no hydroxyl groups, are the most hydrophobic GB-ILs investigated and thus the strongest to promote two-phases. Meanwhile, the hydrophobic character of the [CHES] anion arises from the cyclohexyl group present in its structure (Figure 1), which allows the easiest phase separation.

The hydrophobic character of GBs can be evaluated through their water-octanol partition coefficients, $\log(K_{ow})$. The higher the value of $\log(K_{ow})$ the higher their solubility in the octanol-rich phase and, consequently, the lower the GB polarity. Therefore, higher $\log(K_{ow})$ values correspond to anions that are more easily salted-out and form two-phase systems (ABS). The $\log(K_{ow})$ values of CHES, MES, HEPES, TES, and Tricine are, respectively, 2.04, 0.27, 0.12, -0.51, and -0.69, which is consistent with their phase-forming ability pattern aforementioned.

Figure S4 (Supporting Information) shows a comparison between the effect of $[P_{4444}]^+$ and $[N_{4444}]^+$ [36] on the ABS formation with potassium citrate. It can be seen that $[P_{4444}]^+$ is a better phase forming agent than $[N_{4444}]^+$ for all cation-anion combinations studied in this work. Although both types of compounds are composed of four alkyl chains of similar length, there are also some contributions derived from the central atom. Similar results were obtained in ABS constituted by more conventional ILs and potassium phosphate [41], sodium carbonate [59] and potassium citrate [61] as salting-out agents. In these studies, the results suggested that phosphonium-based ILs are also more effective in promoting ABS when compared with their ammonium-based congeners. Recently, the influence of the cation's central atom of some

ammonium- and phosphonium-based ILs were investigated through experimental and theoretical studies [62]. The authors observed that the ammonium cations are more polar than the corresponding phosphonium-based ILs, which is again consistent with the higher ABS phase-forming ability observed for phosphonium-based GB-ILs.

Extraction of BSA using GB-IL-based ABS

The partition of BSA was studied aiming at understanding its preferential migration towards the GB-IL or salt-rich phases. Table 2 presents the BSA extraction efficiency data obtained for the IL-GB-rich phase at a fixed composition and for which the respective phases' compositions are given in Table S4 in the Supporting Information. From the results presented in Table 2, it is observed that the concentration of BSA is complete (EE_{BSA} = 100%) towards the GB-IL-rich phase, without significant losses of protein, either by precipitation (as already described with other IL-based ABS [63]) or denaturation (conclusion obtained by the mass balance results). The preferential migration of BSA and other macromolecules to the IL-rich phase was already described for other IL- [63-66] and GB-IL-based ABS [54, 67], which could be justified by specific interactions taking place between BSA and the (GB)-ILs [68], although the strong salting-out effect of the salt used cannot be discarded. Despite the results obtained in this and other works [64, 66, 68], in which the protein preferentially migrates to the IL-rich phase, in other works the opposite migration behavior was verified [69, 70].

The stability of the protein conformation when in contact with the $[P_{4444}][GB]$/$[P_{4444}]Cl$ was studied in this work through ATR-FTIR, in particular to determine the protein conformation integrity regarding the secondary structure of proteins [71, 72]. The IR spectra of the amide I group of BSA in presence of (0.05 and 0.5) M of $[P_{4444}][Tricine]$/$[P_{4444}][TES]$/$[P_{4444}][HEPES]$/$[P_{4444}]Cl$ were measured at pH 7.4, since at this pH, these three GB-ILs present good buffer capacity. The

presence of the amide I band is due to carbonyl stretching vibration which appears at ~ 1653 cm^{-1}. In order to analyze the BSA secondary structure, curve fitting was used for the amide I. The bands at (1615, 1631, 1653, 1675, and 1697) cm^{-1} correspond to inter and intra-molecular β-sheets, α-helix, turns, and antiparallel β-sheets, respectively [71, 72]. The α-helix value of BSA in a buffer solution is consistent with those previously reported [73]. The secondary structure of BSA in the studied GB-ILs as well as in the conventional $[P_{4444}]Cl$, is listed in Table 3. The Gaussian curve-fitting analysis of the amide I spectra of BSA in 0.05 M $[P_{4444}]Cl$ and $[P_{4444}][TES]$ are shown in Figure 7, as examples. The α-helices of BSA in GB-ILs are higher than the corresponding GBs. The α-helix contents of BSA in the studied ILs follow the order: $[P_{4444}][TES] > [P_{4444}][HEPES] > [P_{4444}]Cl > [P_{4444}][Tricine]$. It is important to mention that no buffer is used to adjust the pH of the protein solution in the GB-ILs presence, while 0.05 M of HEPES buffer was used for the analysis with the $[P_{4444}]Cl$.

The evaluation of the BSA aggregation in aqueous solutions of ILs is an important factor to be studied to understand the stabilizing/destabilizing effect of the synthesized ILs through proteins. The effect of increasing the concentration of $[P_{4444}][GB]/[P_{4444}]Cl$ on BSA using DLS at pH 7.4 at 25 ºC is presented in Figure 8. The size distribution curves of the studied ILs show that the BSA in the presence of 0.05 M of GB-ILs exhibited two peaks at R_H = 3.7 nm and $R_H \geq 100$ nm. The peak of small particles which appears with a major population is due to the native state of BSA. Meanwhile, the other peak with lower intensity is showing that BSA forms aggregates in these conditions. The size of BSA was increased while increasing the IL concentration from 0.05 M to 0.5 M (Figure 8). This indicates that with the increase of the IL concentration, the BSA molecules aggregate forming oligomeric species. However, these oligomeric species are formed without unfolding as observed from the increase of the α-helices of BSA in the (GB-)ILs.

In order to calculate the binding between $[P_{4444}]Cl$/$[P_{4444}][GB]$ and BSA, the binding model 'quantitative structure-activity relationship (QSAR)-human serum albumin', logK(HSA), was used to predict the binding affinity of $[P_{4444}]Cl$/$[P_{4444}][GB]$ to HSA [74]. This model can be used also to predict the binding of the investigated ILs to BSA because both proteins (HSA and BSA) are similar in terms of their amino acid sequence [75]. The logK(HSA) values of $[P_{4444}]Cl$, $[P_{4444}][TES]$, $[P_{4444}][Tricine]$, and $[P_{4444}][HEPES]$ are, respectively, 0.4438, 0.3112, 0.5754, and 0.8292. These phosphonium-based ILs show a binding affinity to BSA, thus confirming the complete extraction of BSA with no losses as discussed before.

It is well know that BSA has different binding sites for a variety of biomaterials (e.g. fatty acids) with thermal stabilizing effect, [76] where the hydrophobicity and polarity play a significant role in the binding. The polarity of the synthesized ILs can be qualitatively evaluated from the σ-profiles of their ions. The σ-profile is divided into three regions (Figure 9): H-bond donor, H-bond acceptor, and a non-polar region between them. The H-bond cut-off is 0.079 $e \cdot Å^{-2}$, and the hydrogen bonding is the weakest up to 0.01 $e \cdot Å^{-2}$. It is clear from Figure 9 that GB-ILs show strong negative polar peaks over (0.01 to 0.025) $e \cdot Å^{-2}$ (deep red) arising from the oxygen's sulfonic/carboxylic/morpholine groups and hydroxyl groups, as well as, the nitrogen's amine groups, in which they can provide hydrogen bonds with H-bond donor groups such as protein or water. On the other side, only $[P_{4444}][TES]$ shows positive polar peaks at -0.015 $e \cdot Å^{-2}$ (deep blue) arising from one hydroxyl's hydrogen of $[TES]^-$, while the others two hydroxyl's hydrogens formed intramolecular hydrogen bonds with the sulfonic group. The hydroxyl's hydrogens of $[Tricine]^-$ do not show any positive peaks because they form intramolecular hydrogen bonds with themselves and the oxygen's carboxylic group. The hydroxyl's hydrogen of $[HEPES]^-$ forms intramolecular hydrogen bonds with the nearby tertiary amine group. Furthermore, the

amine's hydrogens of $[TES]^-$, $[Tricine]^-$, and $[CHES]^-$ form intramolecular hydrogen bonds with oxygen's sulfonic and carboxylic groups. Therefore, GBs' anions show weak hydrogen bond donor fragments due to the intramolecular hydrogen bond formations. The sharp negative peak of $[P_{4444}]Cl$ is a result of the chloride ion while the broad peak in the non-polar area arises from the aliphatic groups of $[P_{4444}]^+$. This non-polar peak becomes broader in case of GB-ILs due to the methylene groups of the GB's anion, further supporting the higher ability of GB-ILs to form ABS.

Table 4 reports the total mean interaction energy (E_i), electrostatic interaction energy ($E_{i,misfit}$), hydrogen bond interaction energy ($E_{i,HB}$), and van der Waals interaction energy ($E_{i,vdW}$) of the pure GB-ILs derived from COSMO-RS computations. The electrostatic-misfit interaction energy arises from the dissimilarity and mismatching between the hydrogen bond donors and acceptors among ILs ions, as it is evident from the results of the σ-profiles. The data in Table 4 show strongly negative values of van der Waals interaction energy, indicative of their expected strong dispersive interactions with protein. The hydrogen bond energy values are also found to be negative. The electrostatic-misfit contributions are positive due to their lack of H-bond donors, which in turn, show the expected attraction towards the H-donors sites of the protein. The total mean interaction energies of the investigated ILs were found to be negative. Thus, the van der Waals and hydrogen bond interactions between BSA and these ILs play an important role in the protein migration pattern in $[P_{4444}][GB]/[P_{4444}]Cl$-based ABS.

We have previously identified the hydrogen bond interactions between Tricine [36], TES [38], and HEPES [38] anions with BSA using molecular docking. The tricine anion has found to form five hydrogen bonds with Leu346, Glu353, and Arg208 amino acid residues of BSA [36]. TES anion forms two hydrogen bonds with Arg198, while the HEPES anion forms only one hydrogen bond

with Ser 428 [38]. Herein, we also carried out molecular docking to predict the binding sites of MES^-, $CHES^-$, and $[P_{4444}]^+$ to BSA as shown in Figure 10. The MES anion forms three hydrogen bonds with Ser 428, Arg 458, and His 145. CHES anion forms two hydrogen bonds with Arg458 and His145. The residues found next to the $[P_{4444}]^+$ are Thr 190, Ser 428, and Leu 454. The binding free energies of the $[MES]^-$, and $[P_{4444}]^+$ are (-5.0, -5.6, and -5.0) kcal·mol^{-1}, respectively.

Purification of BSA from a bovine serum real sample using GB-IL-based ABS

Proteins are usually present in an original complex media, and in order to evaluate the potential applicability of the IL-based ABS investigated, these systems were applied to purify BSA from a bovine serum real matrix. The GB-ILs-based ABS were evaluated regarding their capacity to extract BSA into the GB-IL-rich phase and to simultaneously remove contaminant macromolecules to the opposite aqueous phase. The analyzed bovine serum sample is mostly composed of two different structural forms of BSA, the monomer (target molecule of this study) and a BSA aggregate (the main contaminant identified in this matrix). Based on the results obtained according to the HPLC chromatograms (Table 5 and Fig. S5 in the Supporting information), and considering the monomer as the target protein, the determined purity of BSA (monomer) in the serum sample is ca. 45 %. Following the same quantification protocol previously applied to study the commercial BSA, the BSA monomer was additionally quantified by SE-HPLC (examples of the chromatograms are shown in Fig. S5 in the Supporting information), indicating that the commercial BSA has a purity of 88 ± 2 %.

As previously observed with the commercial BSA, all GB-IL-based ABS lead to the complete migration of the BSA monomer from the serum samples to the GB-IL-rich phase, i.e. extraction efficiencies of 100%, and as depicted in Fig. S5 in the Supporting Information which confirms that no BSA is detected at the bottom phase. Table 5 depicts the results of extraction efficiency, recovery yield and purity of the BSA monomer at the GB-IL-rich phase. Remarkably, all the studied systems lead to a decrease on the amount of the BSA aggregates at the IL-rich phase, which results in BSA with a higher purification level when compared to the serum sample - the BSA purity increases from 45 ± 2 % to 92 ± 1 %. Moreover, good recovery yields (from 60 to 80%) have been obtained, as presented in Table 5. Thus, GB-IL-based ABS can be seen as potential purification platforms for BSA by eliminating protein aggregates and/or other contaminants from complex matrices.

Toxicities of $[P_{4444}][GB]$ against the marine bacteria *Vibrio fischeri*

To evaluate the ecotoxicity of the five $[P_{4444}][GB]$ ILs, the Microtox® Acute toxicity test [40, 77] was used. Table 6 reports the EC_{50} values determined along with the 95% limits of confidence. The toxic character of $[P_{4444}][GB]$, as well as, that of $[P_{4444}]Cl$ was assessed after 30 minutes of the bacteria exposure, ensuring enough time to verify their effect in the luminescence inhibition [78]. The results show that the $[P_{4444}][GB]$ species present a toxicity that is similar or lower than the toxicity obtained for the $[P_{4444}]Cl$. In this sense, the EC_{50} values can be ranked as follows: $[P_{4444}][MES] > [P_{4444}][HEPES] > [P_{4444}][CHES] > [P_{4444}]Cl$ (the commercial IL) > $[P_{4444}][Tricine] > [P_{4444}][TES]$. This tendency indicates that $[P_{4444}][MES]$ is the most benign compound, while $[P_{4444}][TES]$ is the one with the highest toxicity. The $[P_{4444}][GB]$ (with the exception of $[P_{4444}][TES]$ which belongs to the category "acute 3" – 10 $mg.L^{-1} < EC_{50} \leq 100$ $mg.L^{-1}$) can be classified as non-hazardous substances ($EC_{50} > 100$ $mg.L^{-1}$), according to the

limits imposed by the European Legislation for the aquatic compartment [79]. The trend for the effect of $[GB]^-$ anions on toxicity here observed is in general distinct from that observed before, and for other types of [GB]-ILs [36], suggesting a stronger impact of the $[P_{4444}]^+$ cation. Nevertheless, by finely-tuning the $[GB]^-$ anion, it is possible to design self-buffering $[P_{4444}][GB]$-based ILs with similar or lower toxicity than the non-buffering $[P_{4444}]Cl$.

Conclusions

The synthesis and characterization of new self-buffering ILs, based on the $[P_{4444}]^+$ cation and GB's anions (TES, HEPES, CHES, MES, and Tricine), was here addressed. These ILs demonstrated a high capacity to form ABS with organic salts. In this sense they can be considered as remarkable platforms for the separation and purification of proteins, namely BSA from a bovine serum sample. Moreover, these ILs display an improved environmental benignity (as gauged from the EC_{50} results for *Vibrio fischeri*). The effect of the studied ILs on the BSA structure was investigated using IR absorption spectroscopy, and their binding affinity towards the protein was determined by the QSAR-logK(HSA) model. The $[P_{4444}][GB]$ ILs were found to exhibit a stabilizing effect over the BSA structure as compared with the conventional IL, $[P_{4444}]Cl$. COSMO-RS and molecular docking were also used to address the polarity of the ILs and to better interpret the extraction process. Based on these studies, van der Waals and hydrogen-bonding interactions show to play an important role in the protein partitioning.

Acknowledgements

This work was developed in the scope of the projects CICECO - Aveiro Institute of Materials (Ref. FCT UID/CTM/50011/2013) and PTDC/ATP-EAM/5331/2014, financed by national funds through the FCT/MEC and co-financed by FEDER under the PT2020 Partnership Agreement. Authors are thankful to FCT for financial support through the doctoral and post-doctoral grants of SFRH/BD/94901/2013, and SFRH/BPD/78441/2011 of F.A. e Silva, and M. Taha, respectively. M.G. Freire acknowledges the European Research Council (ERC) for the Grant ERC-2013-StG-337753. S.P.M. Ventura acknowledges FCT for the contract IF/00402/2015 under the *Investigador FCT 2015*.

References

1. Benavides J and Rito-Palomares M, Practical experiences from the development of aqueous two-phase processes for the recovery of high value biological products. *J Chem Technol Biotechnol* **83**: 133-142 (2008).
2. Asenjo JA and Andrews BA, Aqueous two-phase systems for protein separation: A perspective. *J Chromatogr A* **1218**: 8826-8835 (2011).
3. Krishna SH, Srinivas ND, Raghavarao KSMS and Karanth NG, Reverse Micellar Extraction for Downstream Processing of Proteins/Enzymes, in History and Trends in Bioprocessing and Biotransformation, ed by Dutta NN, Hammar F, Haralampidis K, Karanth NG, König A, Krishna SH, Kunze G, Nagy E, Orlich B, Osbourn AE, Raghavarao KSMS, Riedel K, Sahoo GC, Schomäcker R, Srinivas ND and Trojanowska M. Springer Berlin Heidelberg, pp. 119-183 (2002).
4. Pei Y, Wang J, Wu K, Xuan X and Lu X, Ionic liquid-based aqueous two-phase extraction of selected proteins. *Sep Purif Technol* **64**: 288-295 (2009).
5. Freire MG, Claudio AFM, Araujo JMM, Coutinho JAP, Marrucho IM, Lopes JNC and Rebelo LPN, Aqueous biphasic systems: a boost brought about by using ionic liquids. *Chem Soc Rev* **41**: 4966-4995 (2012).

6. Welton T, Room-Temperature Ionic Liquids. Solvents for Synthesis and Catalysis. *Chem Rev* **99**: 2071-2084 (1999).
7. Cantone S, Hanefeld U and Basso A, Biocatalysis in non-conventional media-ionic liquids, supercritical fluids and the gas phase. *Green Chem* **9**: 954-971 (2007).
8. Kumar A and Venkatesu P, Overview of the Stability of α-Chymotrypsin in Different Solvent Media. *Chem Rev* **112**: 4283-4307 (2012).
9. Debeljuh N, Barrow CJ, Henderson L and Byrne N, Structure inducing ionic liquids-enhancement of alpha helicity in the Abeta(1-40) peptide from Alzheimer's disease. *Chem Commun* **47**: 6371-6373 (2011).
10. Lin Huang J, Noss ME, Schmidt KM, Murray L and Bunagan MR, The effect of neat ionic liquid on the folding of short peptides. *Chem Commun* **47**: 8007-8009 (2011).
11. Cláudio AFM, Ferreira AM, Freire CSR, Silvestre AJD, Freire MG and Coutinho JAP, Optimization of the gallic acid extraction using ionic-liquid-based aqueous two-phase systems. *Sep Purif Technol* **97**: 142-149 (2012).
12. Passos H, Sousa ACA, Pastorinho MR, Nogueira AJA, Rebelo LPN, Coutinho JAP and Freire MG, Ionic-liquid-based aqueous biphasic systems for improved detection of bisphenol A in human fluids. *Anal Methods* **4**: 2664-2667 (2012).
13. Pereira JFB, Vicente F, Santos-Ebinuma VC, Araújo JM, Pessoa A, Freire MG and Coutinho JAP, Extraction of tetracycline from fermentation broth using aqueous two-phase systems composed of polyethylene glycol and cholinium-based salts. *Process Biochem* **48**: 716-722 (2013).
14. Du Z, Yu Y-L and Wang J-H, Extraction of Proteins from Biological Fluids by Use of an Ionic Liquid/Aqueous Two-Phase System. *Chem Eur J* **13**: 2130-2137 (2007).
15. Ruiz-Angel MJ, Pino V, Carda-Broch S and Berthod A, Solvent systems for countercurrent chromatography: An aqueous two phase liquid system based on a room temperature ionic liquid. *J Chromatogr A* **1151**: 65-73 (2007).
16. Cao Q, Quan L, He C, Li N, Li K and Liu F, Partition of horseradish peroxidase with maintained activity in aqueous biphasic system based on ionic liquid. *Talanta* **77**: 160-165 (2008).
17. Dreyer S and Kragl U, Ionic liquids for aqueous two-phase extraction and stabilization of enzymes. *Biotech Bioeng* **99**: 1416-1424 (2008).

18. Dreyer S, Salim P and Kragl U, Driving forces of protein partitioning in an ionic liquid-based aqueous two-phase system. *Biochem Eng J* **46**: 176-185 (2009).
19. Pei Y, Li Z, Liu L, Wang J and Wang H, Selective separation of protein and saccharides by ionic liquids aqueous two-phase systems. *Science China Chemistry* **53**: 1554-1560 (2010).
20. Lu Y, Lu W, Wang W, Guo Q and Yang Y, Thermodynamic studies of partitioning behavior of cytochrome c in ionic liquid-based aqueous two-phase system. *Talanta* **85**: 1621-1626 (2011).
21. Deive FJ, Rodriguez A, Pereiro AB, Araujo JMM, Longo MA, Coelho MAZ, Lopes JNC, Esperanca JMSS, Rebelo LPN and Marrucho IM, Ionic liquid-based aqueous biphasic system for lipase extraction. *Green Chem* **13**: 390-396 (2011).
22. Ventura SPM, Sousa SG, Freire MG, Serafim LS, Lima ÁS and Coutinho JAP, Design of ionic liquids for lipase purification. *J Chromatogr B* **879**: 2679-2687 (2011).
23. Ventura SPM, de Barros RLF, de Pinho Barbosa JM, Soares CMF, Lima AS and Coutinho JAP, Production and purification of an extracellular lipolytic enzyme using ionic liquid-based aqueous two-phase systems. *Green Chem* **14**: 734-740 (2012).
24. Deive FJ, Rodríguez A, Rebelo LPN and Marrucho IM, Extraction of Candida antarctica lipase A from aqueous solutions using imidazolium-based ionic liquids. *Sep Purif Technol* **97**: 205-210 (2012).
25. Novak U, Pohar A, Plazl I and Žnidaršič-Plazl P, Ionic liquid-based aqueous two-phase extraction within a microchannel system. *Sep Purif Technol* **97**: 172-178 (2012).
26. Lin X, Wang Y, Zeng Q, Ding X and Chen J, Extraction and separation of proteins by ionic liquid aqueous two-phase system. *Analyst* **138**: 6445-6453 (2013).
27. Zeng Q, Wang Y, Li N, Huang X, Ding X, Lin X, Huang S and Liu X, Extraction of proteins with ionic liquid aqueous two-phase system based on guanidine ionic liquid. *Talanta* **116**: 409-416 (2013).
28. Desai RK, Streefland M, Wijffels RH and H. M. Eppink M, Extraction and stability of selected proteins in ionic liquid based aqueous two phase systems. *Green Chem* (2014).
29. Ding X, Wang Y, Zeng Q, Chen J, Huang Y and Xu K, Design of functional guanidinium ionic liquid aqueous two-phase systems for the efficient purification of protein. *Anal Chim Acta* **815**: 22-32 (2014).

30. Gutiérrez-Arnillas E, Deive FJ, Sanromán MA and Rodríguez A, Ionic liquids for the concomitant use in extremophiles lysis and extremozymes extraction. *Bioresource Technology* **186**: 303-308 (2015).
31. Souza RL, Lima RA, Coutinho JAP, Soares CMF and Lima ÁS, Aqueous two-phase systems based on cholinium salts and tetrahydrofuran and their use for lipase purification. *Separation and Purification Technology* **155**: 118-126 (2015).
32. Souza RL, Ventura SPM, Soares CMF, Coutinho JAP and Lima AS, Lipase purification using ionic liquids as adjuvants in aqueous two-phase systems. *Green Chemistry* **17**: 3026-3034 (2015).
33. Desai RK, Streefland M, Wijffels RH and H. M. Eppink M, Extraction and stability of selected proteins in ionic liquid based aqueous two phase systems. *Green Chemistry* **16**: 2670-2679 (2014).
34. Moreira S, Silvério SC, Macedo EA, Milagres AMF, Teixeira JA and Mussatto SI, Recovery of Peniophora cinerea laccase using aqueous two-phase systems composed by ethylene oxide/propylene oxide copolymer and potassium phosphate salts. *Journal of Chromatography A* **1321**: 14-20 (2013).
35. MacFarlane DR, Vijayaraghavan R, Ha HN, Izgorodin A, Weaver KD and Elliott GD, Ionic liquid "buffers"-pH control in ionic liquid systems. *Chemical Communications* **46**: 7703-7705 (2010).
36. Taha M, e Silva F, Quental MV, Ventura SPM, Freire MG and Coutinho JAP, Good's buffers as a basis for developing self-buffering and biocompatible ionic liquids for biological research. *Green Chem*: 3149–3159. (2014).
37. Taha M, Almeida MR, Silva FAe, Domingues P, Ventura SPM, Coutinho JAP and Freire MG, Novel Biocompatible and Self-buffering Ionic Liquids for Biopharmaceutical Applications. *Chemistry – A European Journal* **21**: 4781-4788 (2015).
38. Taha M, Quental MV, Correia I, Freire MG and Coutinho JAP, Extraction and stability of bovine serum albumin (BSA) using cholinium-based Good's buffers ionic liquids. *Process Biochem* (2015).
39. Taruvai Kalyana Kumar R, De Mello Gindri I, Kinnamon D, Rodrigues DC, Frizzo CP and Prasad S, Use of dicationic ionic liquids as a novel liquid platform for dielectrophoretic cell manipulation. *RSC Advances* **6**: 22594-22603 (2016).

40. Steinberg SM, Poziomek EJ, Engelmann WH and Rogers KR, A review of environmental applications of bioluminescence measurements. *Chemosphere* **30**: 2155-2197 (1995).
41. Louros CLS, Cláudio AFM, Neves CMSS, Freire MG, Marrucho IM, Pauly J and Coutinho JAP, Extraction of Biomolecules Using Phosphonium-Based Ionic Liquids + K3PO4 Aqueous Biphasic Systems. *International Journal of Molecular Sciences* **11**: 1777-1791 (2010).
42. Lee SY, Vicente FA, e Silva FA, Sintra TE, Taha M, Khoiroh I, Coutinho JAP, Show PL and Ventura SPM, Evaluating Self-buffering Ionic Liquids for Biotechnological Applications. *ACS Sustainable Chemistry & Engineering* **3**: 3420-3428 (2015).
43. Gans P and O'Sullivan B, GLEE, a new computer program for glass electrode calibration. *Talanta* **51**: 33-37 (2000).
44. Jameson RF and Wilson MF, Apparent molar ionic products of water in aqueous potassium nitrate solutions and calibration of the glass electrode as a wide-range proton concentration probe. *J Chem Soc, Dalton Trans*: 2607-2610 (1972).
45. Gans P, Sabatini A and Vacca A, Investigation of equilibria in solution. Determination of equilibrium constants with the HYPERQUAD suite of programs. *Talanta* **43**: 1739-1753 (1996).
46. Merchuk JC, Andrews BA and Asenjo JA, Aqueous two-phase systems for protein separation: Studies on phase inversion. *J Chromatogr B* **711**: 285-293 (1998).
47. Klamt A, COSMO-RS from Quantum Chemistry to Fluid Phase Thermodynamics and Drug Design. Elsevier, Amsterdam, The Netherlands (2005).
48. Klamt A and Eckert F, COSMO-RS: a novel and efficient method for the a priori prediction of thermophysical data of liquids. *Fluid Phase Equilib* **172**: 43-72 (2000).
49. Klamt A, Conductor-like Screening Model for Real Solvents: A New Approach to the Quantitative Calculation of Solvation Phenomena. *The Journal of Physical Chemistry* **99**: 2224-2235 (1995).
50. Klamt A, Jonas V, Bürger T and Lohrenz JCW, Refinement and Parametrization of COSMO-RS. *The Journal of Physical Chemistry A* **102**: 5074-5085 (1998).
51. Schafer A, Klamt A, Sattel D, Lohrenz JCW and Eckert F, COSMO Implementation in TURBOMOLE: Extension of an efficient quantum chemical code towards liquid systems. *Physical Chemistry Chemical Physics* **2**: 2187-2193 (2000).

52. Trott O and Olson AJ, AutoDock Vina: Improving the speed and accuracy of docking with a new scoring function, efficient optimization, and multithreading. *J Comp Chem* **31**: 455-461 (2010).

53. Majorek KA, Porebski PJ, Dayal A, Zimmerman MD, Jablonska K, Stewart AJ, Chruszcz M and Minor W, Structural and immunologic characterization of bovine, horse, and rabbit serum albumins. *Mol Immunol* **52**: 174-182 (2012).

54. Taha M, Quental MV, Correia I, Freire MG and Coutinho JAP, Extraction and stability of bovine serum albumin (BSA) using cholinium-based Good's buffers ionic liquids. *Process Biochemistry* **50**: 1158-1166 (2015).

55. Environmental A, Microtox manual. *Carlbad CA, USA* (1998).

56. Goldberg RN, Kishore N and Lennen RM, Thermodynamic Quantities for the Ionization Reactions of Buffers. *J Phys Chem Ref Data* **31**: 231-370 (2002).

57. Alderighi L, Gans P, Ienco A, Peters D, Sabatini A and Vacca A, Hyperquad simulation and speciation (HySS): a utility program for the investigation of equilibria involving soluble and partially soluble species. *Coord Chem Rev* **184**: 311-318 (1999).

58. Freire MG, Claudio AFM, Araujo JMM, Coutinho JAP, Marrucho IM, Lopes JNC and Rebelo LPN, Aqueous biphasic systems: a boost brought about by using ionic liquids. *Chemical Society Reviews* **41**: 4966-4995 (2012).

59. Marques CF, Mourao T, Neves CM, Lima AS, Boal-Palheiros I, Coutinho JA and Freire MG, Aqueous biphasic systems composed of ionic liquids and sodium carbonate as enhanced routes for the extraction of tetracycline. *Biotechnol Prog* **29**: 645-654 (2013).

60. Pegram LM and Record MT, Hofmeister Salt Effects on Surface Tension Arise from Partitioning of Anions and Cations between Bulk Water and the Air−Water Interface. *The Journal of Physical Chemistry B* **111**: 5411-5417 (2007).

61. Passos H, Ferreira AR, Cláudio AFM, Coutinho JAP and Freire MG, Characterization of aqueous biphasic systems composed of ionic liquids and a citrate-based biodegradable salt. *Biochemical Engineering Journal* **67**: 68-76 (2012).

62. Carvalho PJ, Ventura SPM, Batista MLS, Schröder B, Gonçalves F, Esperança J, Mutelet F and Coutinho JAP, Understanding the impact of the central atom on the ionic liquid behavior: Phosphonium vs ammonium cations. *The Journal of Chemical Physics* **140**: - (2014).

63. Pereira MM, Pedro SN, Quental MV, Lima ÁS, Coutinho JAP and Freire MG, Enhanced extraction of bovine serum albumin with aqueous biphasic systems of phosphonium- and ammonium-based ionic liquids. *Journal of Biotechnology* **206**: 17-25 (2015).

64. Song CP, Ramanan RN, Vijayaraghavan R, MacFarlane DR, Chan E-S and Ooi C-W, Green, Aqueous Two-Phase Systems Based on Cholinium Aminoate Ionic Liquids with Tunable Hydrophobicity and Charge Density. *ACS Sustainable Chemistry & Engineering* **3**: 3291-3298 (2015).

65. Deive FJ, Rodríguez A, Rebelo LPN and Marrucho IM, Extraction of Candida antarctica lipase A from aqueous solutions using imidazolium-based ionic liquids. *Separation and Purification Technology* **97**: 205-210 (2012).

66. Bai Z, Chao Y, Zhang M, Han C, Zhu W, Chang Y, Li H and Sun Y, Partitioning Behavior of Papain in Ionic Liquids-Based Aqueous Two-Phase Systems. *Journal of Chemistry* **2013**: 6 (2013).

67. Taha M, e Silva FA, Quental MV, Ventura SPM, Freire MG and Coutinho JAP, Good's buffers as a basis for developing self-buffering and biocompatible ionic liquids for biological research. *Green Chemistry* **16**: 3149-3159 (2014).

68. Ventura SPM and Coutinho JAP, Chapter 3 - Lipase Production and Purification from Fermentation Broth Using Ionic Liquids A2 - Xu, Xuebing, in Ionic Liquids in Lipid Processing and Analysis, ed by Guo Z and Cheong L-Z. AOCS Press, pp. 59-97 (2016).

69. Ventura SPM, de Barros RLF, de Pinho Barbosa JM, Soares CMF, Lima AS and Coutinho JAP, Production and purification of an extracellular lipolytic enzyme using ionic liquid-based aqueous two-phase systems. *Green Chemistry* **14**: 734-740 (2012).

70. Ventura SPM, Sousa SG, Freire MG, Serafim LS, Lima ÁS and Coutinho JAP, Design of ionic liquids for lipase purification. *Journal of Chromatography B* **879**: 2679-2687 (2011).

71. Seshadri S, Khurana R and Fink AL, [36] Fourier transform infrared spectroscopy in analysis of protein deposits, in Methods in Enzymology. Academic Press, pp. 559-576 (1999).

72. Shivu B, Seshadri S, Li J, Oberg KA, Uversky VN and Fink AL, Distinct β-Sheet Structure in Protein Aggregates Determined by ATR–FTIR Spectroscopy. *Biochemistry* **52**: 5176-5183 (2013).

73. Ghosh S, Jana S and Guchhait N, Domain Specific Association of Small Fluorescent Probe trans-3-(4-Monomethylaminophenyl)-Acrylonitrile (MMAPA) with Bovine Serum Albumin (BSA) and Its Dissociation from Protein Binding Sites by Ag Nanoparticles: Spectroscopic and Molecular Docking Study. *J Phys Chem B* **116**: 1155-1163 (2011).

74. Xue CX, Zhang RS, Liu HX, Yao XJ, Liu MC, Hu ZD and Fan BT, QSAR Models for the Prediction of Binding Affinities to Human Serum Albumin Using the Heuristic Method and a Support Vector Machine. *J Chem Inf Comput Sci* **44**: 1693-1700 (2004).

75. Benyamini H, Shulman-Peleg A, Wolfson HJ, Belgorodsky B, Fadeev L and Gozin M, Interaction of C60-Fullerene and Carboxyfullerene with Proteins: Docking and Binding Site Alignment. *Bioconjugate Chem* **17**: 378-386 (2006).

76. Michnik A, Michalik K and Drzazga Z, Stability of bovine serum albumin at different pH. *J Therm Anal Calorim* **80**: 399-406 (2005).

77. Corporation M, Microtox® manual—a toxicity testing handbook. *Microtox® manual—a toxicity testing handbook Microbics Corporation* **Carlsbad**: 1–5 (1992).

78. Ventura SPM, Marques CS, Rosatella AA, Afonso CAM, Gonçalves F and Coutinho JAP, Toxicity assessment of various ionic liquid families towards Vibrio fischeri marine bacteria. *Ecotoxicol Environ Saf* **76**: 162-168 (2012).

79. Li L, Xie J, Yu S, Su Z, Liu S, Liu F, Xie C and Zhang B, Novel compatible system of [C2OHmim][OAc]-cellulases for the in situ hydrolysis of lignocellulosic biomass. *RSC Adv* **2**: 11712-11718 (2012).

Tables

Table 1. Protonation constants of GB/GB-ILs in water at 25 °C and I = 0.1 M of $NaNO_3$

GB/GB-ILs	pKa_1	SD [a]	pKa_2	SD [a]
MES	2.28	0.07	6.12 (6.07) [b]	0.02
$[P_{4444}][MES]$	2.21	0.10	5.91	0.06
TES	3.05	0.02	7.30 (7.42) [b]	0.01
$[P_{4444}][TES]$	—	—	7.21	0.03
Tricine	2.68 (2.40)[b]	0.03	8.08 (8.00) [b]	0.02
$[P_{4444}][Tricine]$	2.39	0.05	7.82	0.01
HEPES	3.17 (3.0) [b]	0.04	7.35 (7.45) [b]	0.04
$[P_{4444}][HEPES]$	2.77	0.10	7.23	0.02
CHES	1.76	0.03	9.13	0.01
$[P_{4444}][CHES]$	—	—	8.93	0.05

[a] Standard deviation. [b] Reference [56].

Table 2. Extraction efficiency of BSA, EE_{BSA} (%) obtained when the ABS composed of $[P_{4444}][GB]$ + $K_3C_6H_5O_7$ at 25 ºC at different mixture compositions was applied.

GB-ILs/ILs	weight fraction composition (wt %)		EE_{BSA} (± 5%)
	IL	$K_3C_6H_5O_7$	
$[P_{4444}][Tricine]$	38.76	15.02	100
$[P_{4444}][HEPES]$	39.45	13.74	100
$[P_{4444}][CHES]$	38.08	13.55	100
$[P_{4444}][MES]$	38.98	16.30	100
$[P_{4444}][TES]$	39.52	14.43	100
$[P_{4444}]Cl$	38.91	13.99	100

Table 3. Secondary structure analysis (infrared spectra) of BSA in conventional $[P_{4444}][GBs]/[P_{4444}]Cl$ at pH 7.4.

Amide I components	**TES 0.05 M**	**HEPES 0.05 M**	**Tricine 0.05 M**	**$[P_{4444}]Cl$**		**$[P_{4444}][TES]$**		**$[P_{4444}][HEPES]$**		**$[P_{4444}][Tricine]$**	
				0.05 M	**0.5 M**	**0.05 M**	**0.5 M**	**0.05 M**	**0.5 M**	**0.05 M**	**0.5 M**
Inter β-sheet	—	—	2.4[b]	—	—	—	—	—	—	—	—
Intra β-sheet	24.3[a]	26.4[a]	25.0[b]	28.8	29.7	25.7	24.3	25.4	25.8	24.4	23.6
α-helix	59.8[a]	58.3[a]	57.6[b]	60.6	61.2	64.9	65.9	61.2	62.9	59.9	60.5
turn	15.9[a]	25.3[a]	14.2[b]	10.6	9.1	9.4	9.8	13.4	11.3	15.7	15.9
antiparallel β-sheet	—	—	0.8[b]	—	—	—	—	—	—	—	—

[a] Reference [38]
[b] Reference [36]

[#] both authors contributed equally for the development of this work

*Corresponding author. Fax: +351 234 370 084.
E-mail: jcoutinho@ua.pt (J.A.P. Coutinho).

Table 4. Interaction energies of $[P_{4444}][GB]/[P_{4444}]Cl$ at 25 °C.

$[P_{4444}][GB]/[P_{4444}]Cl$	E_i	$E_{i,MF}$	$E_{i,HB}$	$E_{i,vdW}$
			kcal·mol^{-1}	
$[P_{4444}]Cl$	-6.75	16.25	-2.38	-20.62
$[P_{4444}]^+$	-8.20	10.75	-1.20	-17.75
Cl	1.45	5.50	-1.18	-2.87
$[P_{4444}][Tricine]$	-12.78	14.11	-2.22	-24.67
$[P_{4444}]^+$	-9.65	8.04	-1.07	-16.62
$[Tricine]^-$	-3.13	6.07	-1.15	-8.05
$[P_{4444}][TES]$	-18.75	12.23	-5.31	-25.68
$[P_{4444}]^+$	-10.26	7.04	-0.72	-16.58
$[TES]^-$	-8.49	5.19	-4.59	-9.10
$[P_{4444}][HEPES]$	-13.25	16.43	-2.04	-27.64
$[P_{4444}]^+$	-9.49	8.27	-1.00	-16.76
$[HEPES]^-$	-3.76	8.16	-1.04	-10.88
$[P_{4444}][MES]$	-11.51	16.08	-1.95	-25.64
$[P_{4444}]^+$	-9.19	8.55	-0.98	-16.77
$[MES]^-$	-2.32	7.53	-0.97	-8.873
$[P_{4444}][CHES]$	-14.71	14.39	-1.95	-27.16
$[P_{4444}]^+$	-10.05	7.77	-0.98	-16.84
$[CHES]^-$	-4.66	6.62	-0.97	-10.32

[#] both authors contributed equally for the development of this work

*Corresponding author. Fax: +351 234 370 084.
E-mail: jcoutinho@ua.pt (J.A.P. Coutinho).

Table 5. Extraction efficiency of monomeric BSA, EE_{BSA} (%), BSA purity, P_{BSA} (%), and BSA recovery yield, Y_{BSA} (%), from a bovine serum sample, applying ABS composed of $[P_{4444}][GB]$ + $C_6H_5K_3O_7$ + H_2O at 25 °C.

System	EE_{BSA} (± 5) %	$P_{BSA} \pm \sigma$ (%)	$Y_{BSA} \pm \sigma$ (%)
$[P_{4444}][Tricine]$	100	92 ± 1	80.1 ± 0.7
$[P_{4444}][TES]$	100	89 ± 2	73.1 ± 0.3
$[P_{4444}][HEPES]$	100	75.0 ± 0.3	69 ± 7
$[P_{4444}][CHES]$	100	86 ± 2	64.2 ± 0.5
$[P_{4444}][MES]$	100	85 ± 2	59.4 ± 0.8
Serum sample	–	45 ± 2	–
Commercial BSA	–	88 ± 2	–

Table 6. EC_{50} values after 30 minutes of exposure time with the 95% confidence limits (within brackets) for $[P_{4444}][GB]$ and $[P_{4444}]Cl$.

Compound	EC_{50} (mg L^{-1}) at 30 min (lower limit; upper limit)
$[P_{4444}]Cl$	110.26 (96.57; 123.95)
$[P_{4444}][MES]$	231.25 (204.72; 257.78)
$[P_{4444}][TES]$	85.98 (72.48; 99.48)
$[P_{4444}][CHES]$	154.31 (137.56; 171.07)
$[P_{4444}][Tricine]$	107.82 (86.08; 129.55)
$[P_{4444}][HEPES]$	185.58 (174.07; 197.10)

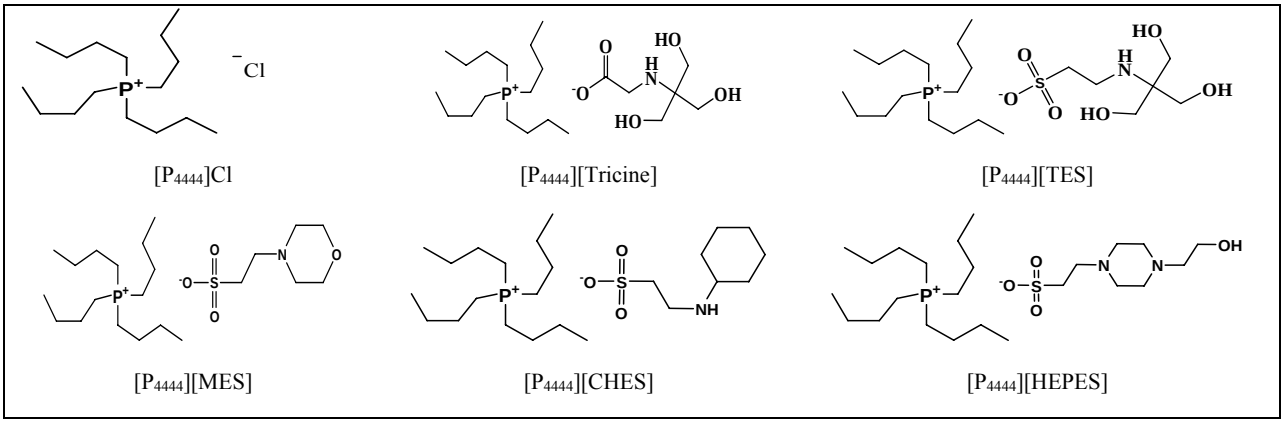

Figure 1. Chemical structure of the studied $[P_{4444}]Cl$/$[P_{4444}][GB]$.

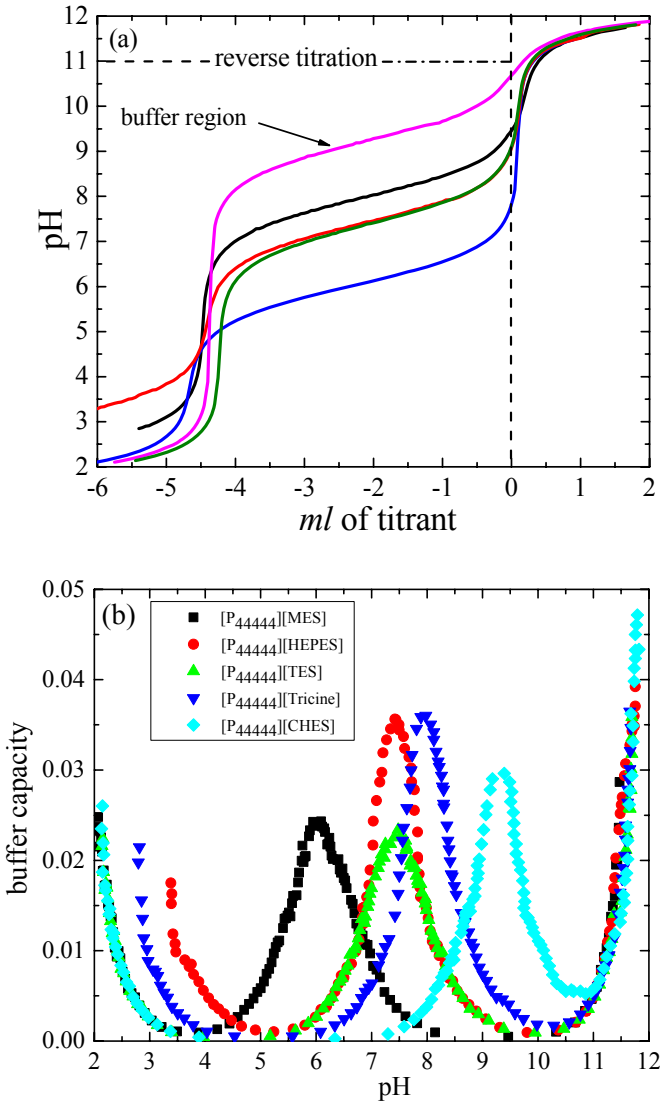

Figure 2. (a) Plots of pH *vs.* mL of 0.1 mol·dm^{-3} of NaOH/HCl added to 10.0 ml of 0.05 mol·dm^{-3} of GB-IL ([P_{4444}][MES] (blue line), [P_{4444}][TES] (olive line), [P_{4444}][HEPES] (red line), [P_{4444}][CHES] (magenta line), and [P_{4444}][Tricine] (black line) in water at (25.0 ± 0.1) °C; the reverse titration region is for mL of 0.1 mol·dm^{-3} of HCI added to 10.0 mL of 0.05 mol·dm^{-3} of GB-IL. (b) Buffer capacity as a function of pH for 0.05 M of GB-IL titrated with 0.1 mol·dm^{-3} of HCl/NaOH at (25.0 ± 0.1) °C.

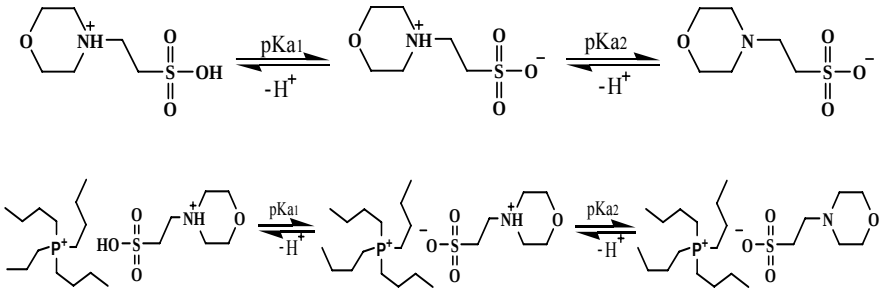

Figure 3. Protonation equilibria of MES and [P_{4444}][MES].

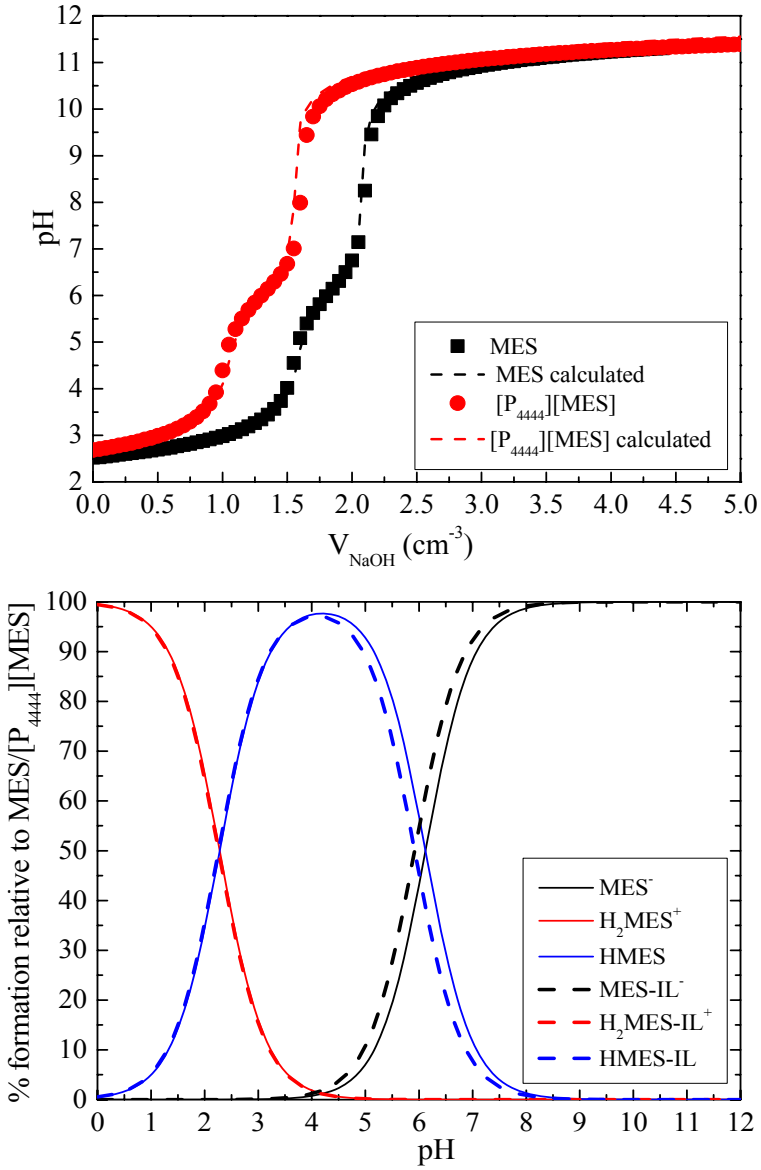

Figure 4. (a) pH titration curves of $1 \cdot 10^{-3}$ M of MES and $[P_{4444}][MES]$ at 25 °C and $I = 0.1$ M of $NaNO_3$. The dashed lines are the calculated pH from the refinement operations. (b) Species-distribution diagrams of $1 \cdot 10^{-3}$ M of MES and $[P_{4444}][MES]$ at 25 °C and $I = 0.1$ M of $NaNO_3$.

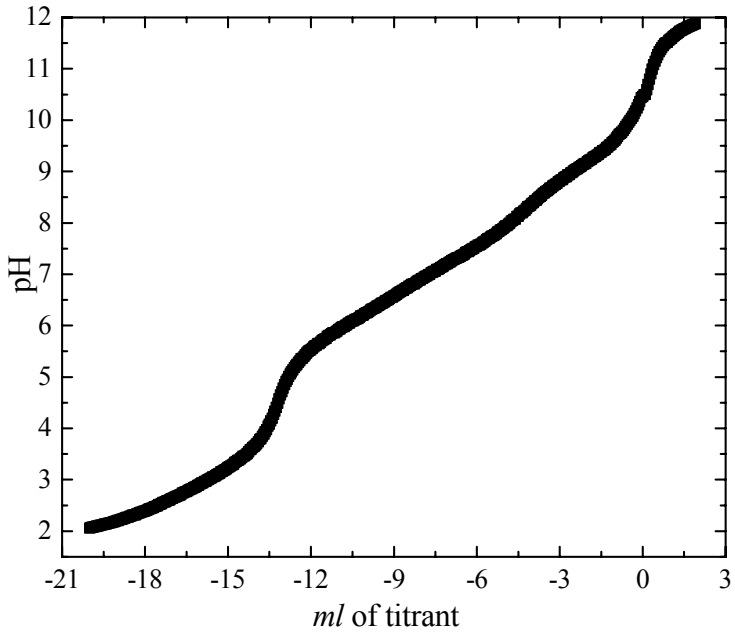

Figure 5. Plots of pH *vs.* mL of 0.1 mol·dm^{-3} of NaOH/HCl added to a mixture of 10.0 ml of 0.05 mol·dm^{-3} '[P_{4444}][MES]+[P_{4444}][HEPES]+ [P_{4444}][CHES]' at (25.0 ± 0.1) °C.

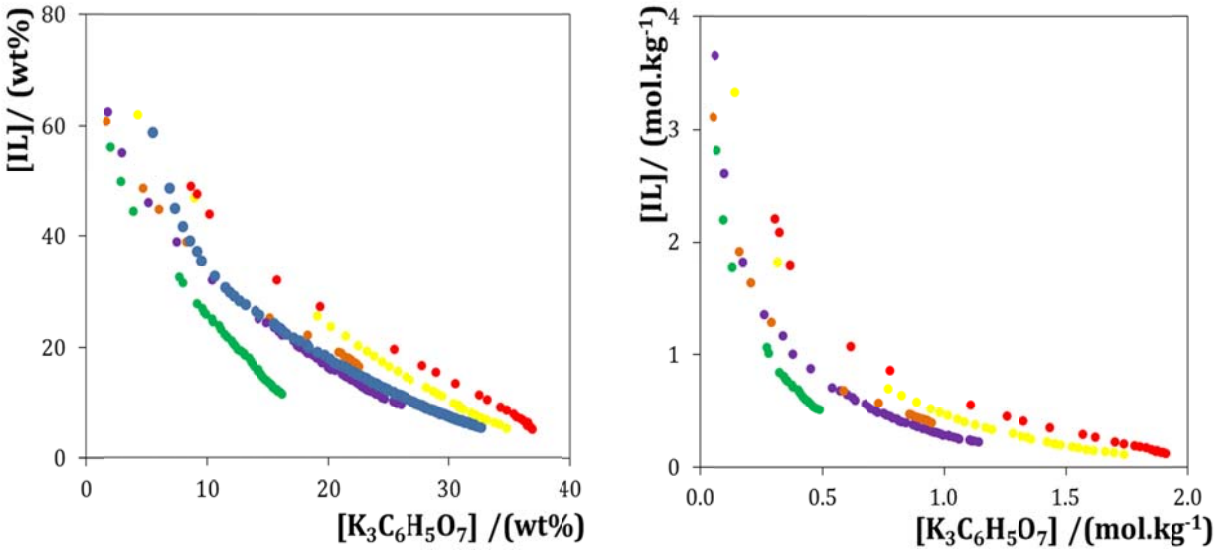

Figure 6. Ternary phase diagrams for the systems composed of IL + $K_3C_6H_5O_7$ + water at 25 °C and atmospheric pressure in wt% (left) and in mol.kg-1 (right): (●) $[P_{4444}][Tricine]$, (●) $[P_{4444}][MES]$, (●) $[P_{4444}][HEPES]$, (●) $[P_{4444}][TES]$, (●) $[P_{4444}][CHES]$, and (●) $[P_{4444}]Cl$ [61].

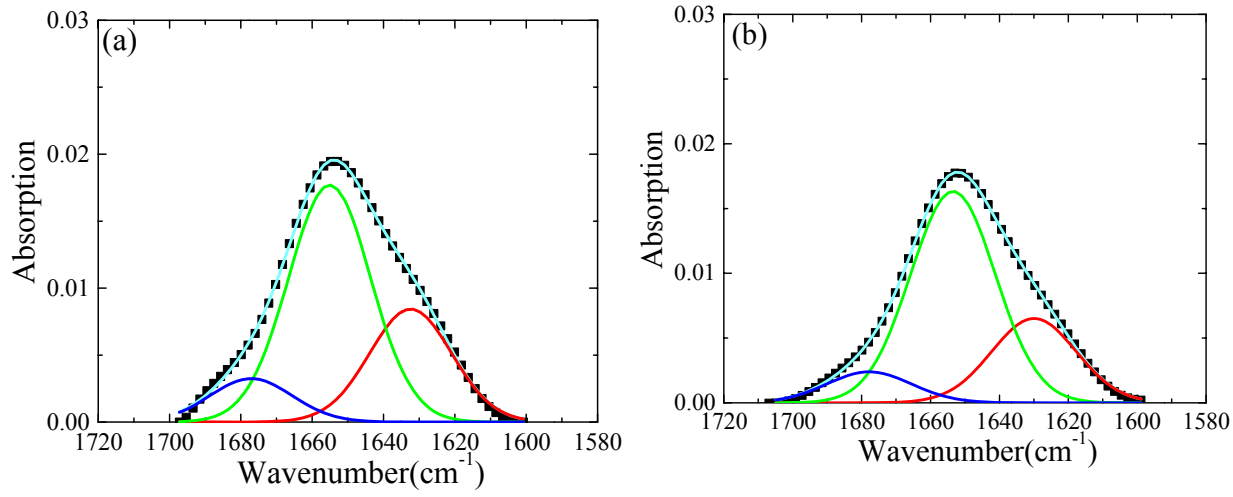

Figure 7. Gaussian curve-fitting analysis of amide I spectra of BSA in 0.05 M of $[P_{4444}]Cl$ (a) and in 0.05 M of $[P_{4444}][TES]$ at pH 7.4.

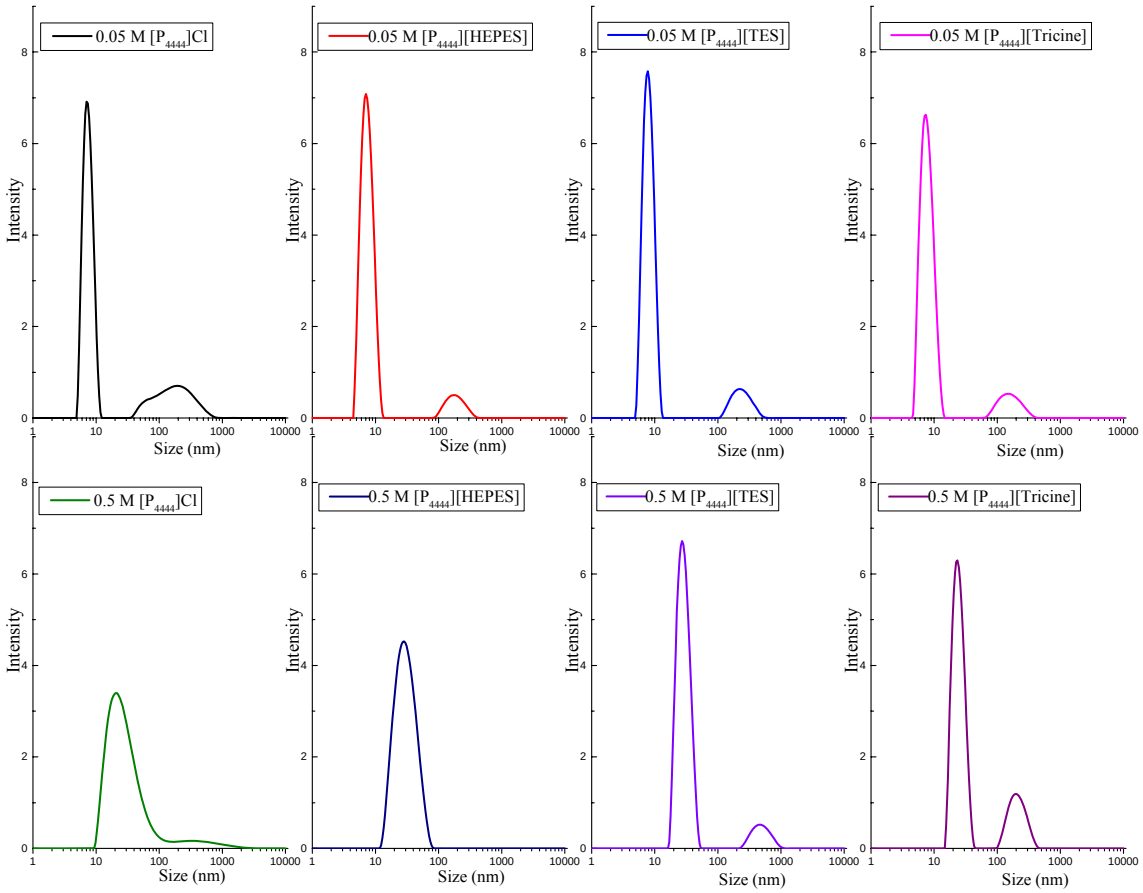

Figure 8. The intensity distribution graph of BSA in (0.05 and 0.5) M of $[P_{4444}]Cl$/$[P_{4444}][TES]$/ $[P_{4444}][Tricine]$/$[P_{4444}][HEPES]$, at pH 7.4 and 25 ºC.

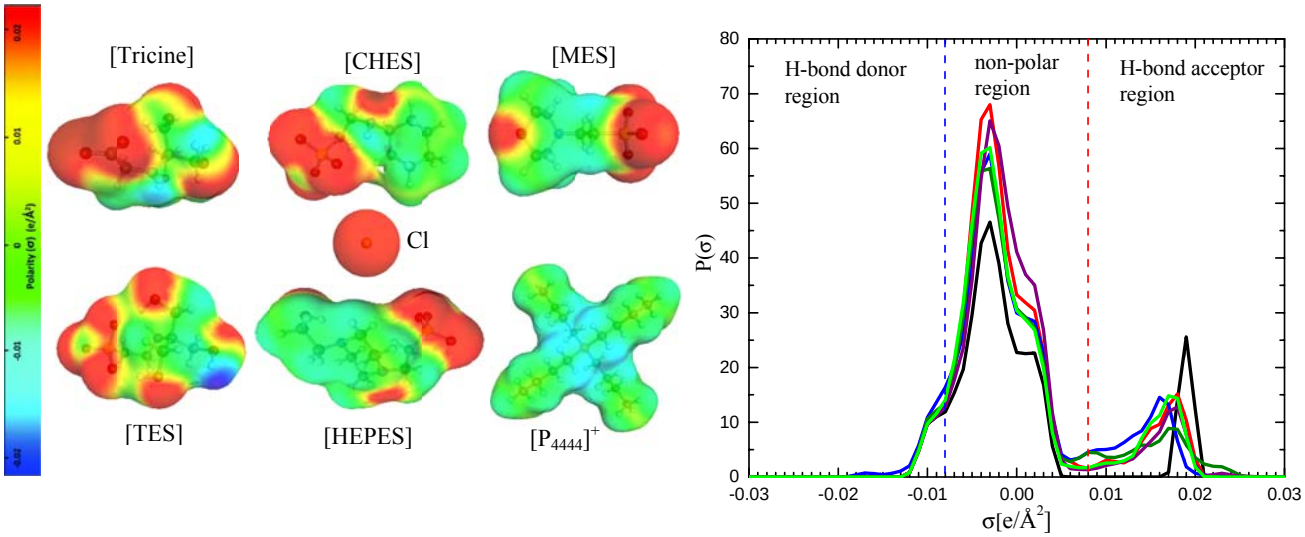

Figure 9. σ-profiles of $[P_{4444}]Cl$ (black line), $[P_{4444}][HEPES]$ (red line), $[P_{4444}][TES]$ (blue line), $[P_{4444}][Tricine]$ (olive line), $[P_{4444}][CHES]$ (purple line), and $[P_{4444}][MES]$ (green line).

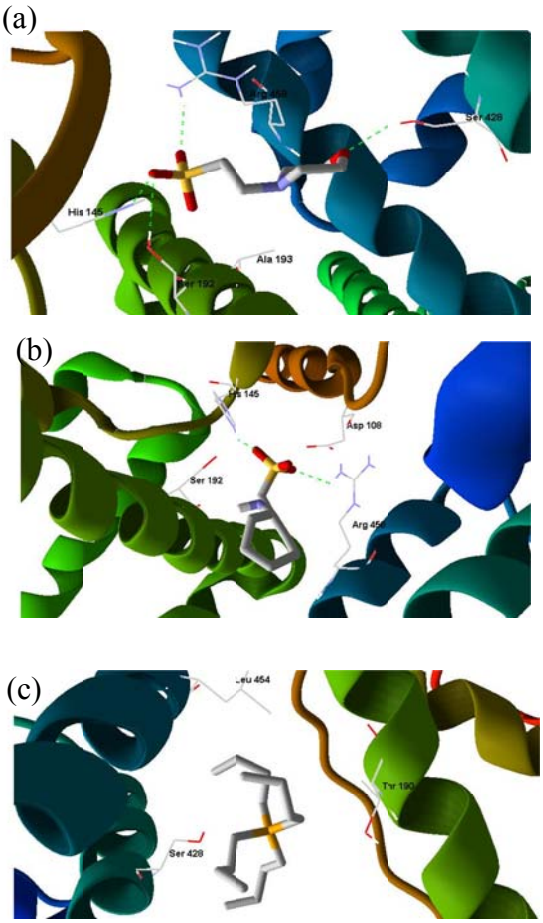

Figure 10. Molecular docking of BSA with $[MES]^-$ (a), $[CHES]^-$ (b), and $[P_{4444}]^+$ (c).